Hindawi
Mathematical Problems in Engineering
Volume 2019, Article ID 3128356, 15 pages
https://doi.org/10.1155/2019/3128356

Research Article

An LMI-Based Simple Robust Control for Load Sway Rejection of Rotary Cranes with Double-Pendulum Effect

Huimin Ouyang, Jian Wang, Guangming Zhang, Lei Mei, and Xin Deng

College of Electrical Engineering and Control Science, Nanjing Tech University, No. 30 Puzhu Road(s), Nanjing 211816, China

Correspondence should be addressed to Huimin Ouyang; ouyang1982@njtech.edu.cn

Received 9 October 2018; Revised 12 November 2018; Accepted 21 January 2019; Published 11 February 2019

Academic Editor: Ning Sun

In the double-pendulum rotary crane case, the load sway properties become more complicated so that the difficulty of design and analysis of crane control system is increased. Moreover, the change of rope length not only affects the stability of the system, but also leads to the decline of control performance. In order to solve the foregoing problems, a simple model for controller design is obtained by linearizing and decoupling the complex nonlinear model of rotary crane. Then, a linear feedback controller which can furnish robust performance is presented. Finally, numerical simulations verify the effectiveness of the proposed method by comparing with a traditional approach.

1. Introduction

As a kind of handling robot, the crane systems have the advantages of less executive mechanism and simple structure; therefore, they have been widely used in various production departments [1]. However, load sways caused by the cart or boom motion not only damage goods, reduce production efficiency, but also cause accidents, even casualties. Hence, how to design a control method that can effectively suppress the load sways has been a hot and difficult point in both academic and industrial circles.

Until now, various approaches were applied to crane systems [2–26]. Nonetheless, when the hook mass or load shape cannot be ignored, the load swing presents two-stage swing. For this problem, open-loop methods such as input shaping technology [27–32], motion planning method [33, 34], were presented. On the other hand, closed-loop methods were also reported in [35, 36]. Furthermore, an input-shaping-based SIRMs fuzzy approach was reported in [37]. Ouyang et al. reported two novel sliding-mode based approaches and a simple LMI-based robust method [38–40]. A nonlinear quasi-PID scheme and an adaptive nonlinear controller were applied to overhead cranes in [41, 42].

In conclusion, although open-loop approaches were introduced in [27–34], accurate crane models were always needed. On the other hand, too complicated algorithms were adopted in [35–42] to achieve good robust or adaptive performance. Moreover, different from the load sways of double-pendulum overhead cranes which were dealt with in the most existing literatures [27–42], the double pendulums in the rotary crane system are both conical pendulums, and the system characteristics are more complex. Hence, even if the similar algorithm shown in [38] is adopted, the method for calculating the controller gain is different. Moreover, as far as we know, there are few related reports on the load sway suppression control of rotary cranes with double-pendulum effect.

In order to solve the foregoing problems, a simple model for controller design is obtained by linearizing and decoupling the complex nonlinear model of rotary crane. Next, a linear feedback controller which can furnish robust performance is presented. The controller gains are obtained by using synthesizing a pole placement and a optimal regulator problems [43]. Finally, numerical simulations verify the effectiveness of the proposed method by comparing with a traditional approach.

2. Rotary Crane Dynamics

Figure 1 shows the model of a rotary crane with double-pendulum effect [30]:

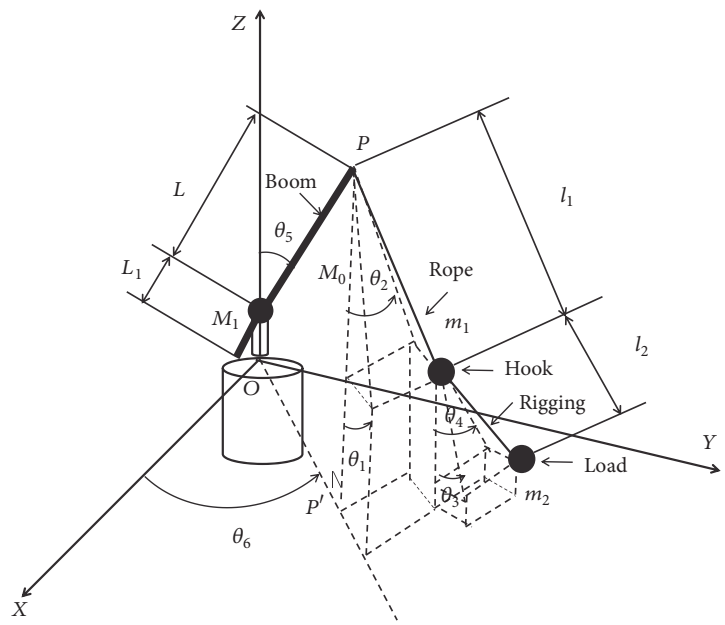

Figure 1: Rotary crane model.

$$
\begin{aligned}
&(m_1+m_2)\,l_1^2\left(1+\theta_1^2\right)\ddot{\theta}_1+(m_1+m_2)\,l_1^2\theta_1\theta_2\ddot{\theta}_2\\
&\quad+m_2l_1l_2\left(1+\theta_1\theta_3\right)\ddot{\theta}_3+m_2l_1l_2\theta_1\theta_4\ddot{\theta}_4+(m_1+m_2)\\
&\quad\cdot l_1L\left(C_5-\theta_1S_5\right)\ddot{\theta}_5-\left((m_1+m_2)\,l_1^2\theta_2+m_2l_1l_2\theta_4\right)\\
&\quad\cdot\ddot{\theta}_6+(m_1+m_2)\,l_1^2\theta_1\dot{\theta}_1^2+\left((m_1+m_2)\,l_1^2\theta_1\right.\\
&\quad\left.-2\,(m_1+m_2)\,l_1^2\dot{\theta}_6\right)\dot{\theta}_2+m_2l_1l_2\theta_1\dot{\theta}_3^2+\left(m_2l_1l_2\theta_1\dot{\theta}_4\right.\\
&\quad\left.-2m_2l_1l_2\dot{\theta}_6\right)\dot{\theta}_4-(m_1+m_2)\,l_1L\left(S_5+\theta_1C_5\right)\dot{\theta}_5^2\\
&\quad-\left((m_1+m_2)\,l_1^2\theta_1+m_2l_1l_2\theta_3+(m_1+m_2)\,l_1LS_5\right)\dot{\theta}_6^2\\
&\quad+(m_1+m_2)\,l_1g\theta_1=0
\end{aligned}
\tag{1}
$$

$$
\begin{aligned}
&(m_1+m_2)\,l_1^2\theta_1\theta_2\ddot{\theta}_1+(m_1+m_2)\,l_1^2\left(1+\theta_2^2\right)\ddot{\theta}_2\\
&\quad+m_2l_1l_2\theta_2\theta_3\ddot{\theta}_3+m_2l_1l_2\left(1+\theta_2\theta_4\right)\ddot{\theta}_4-(m_1+m_2)\\
&\quad\cdot l_1L\theta_2S_5\ddot{\theta}_5+\left((m_1+m_2)\,l_1^2\theta_1+(m_1+m_2)\,l_1LS_5\right.\\
&\quad\left.+m_2l_1l_2\theta_3\right)\ddot{\theta}_6+\left((m_1+m_2)\,l_1^2\theta_2\dot{\theta}_1\right.\\
&\quad\left.+2\,(m_1+m_2)\,l_1^2\dot{\theta}_6\right)\dot{\theta}_1+(m_1+m_2)\,l_1^2\theta_2\dot{\theta}_2^2\\
&\quad+\left(m_2l_1l_2\theta_2\dot{\theta}_3+2m_2l_1l_2\dot{\theta}_6\right)\dot{\theta}_3+m_2l_1l_2\theta_2\dot{\theta}_4^2\\
&\quad+\left(2\,(m_1+m_2)\,l_1LC_5\dot{\theta}_6-(m_1+m_2)\,l_1L\theta_2C_5\dot{\theta}_5\right)\dot{\theta}_5\\
&\quad-\left((m_1+m_2)\,l_1^2\theta_2+m_2l_1l_2\theta_4\right)\dot{\theta}_6^2+(m_1+m_2)\,l_1g\theta_2\\
&\quad=0
\end{aligned}
\tag{2}
$$

$$
\begin{aligned}
&m_2l_1l_2\left(1+\theta_1\theta_3\right)\ddot{\theta}_1+m_2l_1l_2\theta_2\theta_4\ddot{\theta}_2+m_2l_2^2\left(1+\theta_3^2\right)\ddot{\theta}_3\\
&\quad+m_2l_2^2\theta_3\theta_4\ddot{\theta}_4+m_2l_2L\left(C_5-\theta_3S_5\right)\ddot{\theta}_5-\left(m_2l_2^2\theta_4\right.\\
&\quad\left.+m_2l_1l_2\theta_2\right)\ddot{\theta}_6+m_2l_1l_2\theta_3\dot{\theta}_1^2+\left(m_2l_1l_2\theta_3\dot{\theta}_2\right.\\
&\quad\left.-2m_2l_1l_2\dot{\theta}_6\right)\dot{\theta}_2+m_2l_2^2\theta_3\dot{\theta}_3^2+\left(m_2l_2^2\theta_3\dot{\theta}_4\right.\\
&\quad\left.-2m_2l_2^2\dot{\theta}_6\right)\dot{\theta}_4-m_2l_2L\left(S_5+\theta_3C_5\right)\dot{\theta}_5^2-\left(m_2l_2^2\theta_3\right.\\
&\quad\left.+m_2l_1l_2\theta_1+m_2l_2LS_5\right)\dot{\theta}_6^2+m_2l_2g\theta_3=0
\end{aligned}
\tag{3}
$$

$$
\begin{aligned}
&m_2l_1l_2\theta_1\theta_4\ddot{\theta}_1+m_2l_1l_2\left(1+\theta_2\theta_4\right)\ddot{\theta}_2+m_2l_2^2\theta_3\theta_4\ddot{\theta}_3\\
&\quad+m_2l_2^2\left(1+\theta_4^2\right)\ddot{\theta}_4-m_2l_2L\theta_4S_5\ddot{\theta}_5+\left(m_2l_2^2\theta_3\right.\\
&\quad\left.+m_2l_2LS_5+m_2l_1l_2\theta_1\right)\ddot{\theta}_6+\left(m_2l_1l_2\theta_4\dot{\theta}_1\right.\\
&\quad\left.+2m_2l_1l_2\dot{\theta}_6\right)\dot{\theta}_1+m_2l_1l_2\theta_4\dot{\theta}_2^2+\left(m_2l_2^2\theta_4\dot{\theta}_3\right.\\
&\quad\left.+2m_2l_2^2\dot{\theta}_6\right)\dot{\theta}_3+m_2l_2^2\theta_4\dot{\theta}_4^2+\left(2m_2l_2LC_5\dot{\theta}_6\right.\\
&\quad\left.-m_2l_2L\theta_4C_5\dot{\theta}_5\right)\dot{\theta}_5-\left(m_2l_1l_2\theta_2+m_2l_2^2\theta_4\right)\dot{\theta}_6^2\\
&\quad+m_2l_2g\theta_4=0
\end{aligned}
\tag{4}
$$

$$
\begin{aligned}
&(m_1+m_2)\,l_1L\left(C_5-\theta_1S_5\right)\ddot{\theta}_1-(m_1+m_2)\,l_1L\theta_2S_5\ddot{\theta}_2\\
&\quad+m_2l_2L\left(C_5-\theta_3S_5\right)\ddot{\theta}_3-m_2l_2L\theta_4S_5\ddot{\theta}_4\\
&\quad+\left((m_1+m_2)\,L^2+I_y+J_5\right)\ddot{\theta}_5\\
&\quad-\left((m_1+m_2)\,l_1L\theta_2C_5+m_2l_2L\theta_4C_5\right)\ddot{\theta}_6-(m_1
\end{aligned}
$$

$$
\begin{aligned}
&+ m_2) l_1 L S_5 \dot{\theta}_1^2 - (m_1 + m_2) l_1 L S_5 \dot{\theta}_2^2 - m_2 l_2 L S_5 \dot{\theta}_3^2 \\
&- m_2 l_2 L S_5 \dot{\theta}_4^2 - \left(2 (m_1 + m_2) l_1 L C_5 \dot{\theta}_2 \right. \\
&\left. + 2 m_2 l_2 L C_5 \dot{\theta}_4 + (m_1 + m_2) l_1 L \theta_1 C_5 \dot{\theta}_6 \right) \dot{\theta}_6 \\
&- g S_5 \left(\frac{1}{2} M_0 L + (m_1 + m_2) L - \frac{1}{2} M_1 L_1 \right) \\
&- \frac{1}{2} \left((m_1 + m_2) L^2 + I_x - I_z \right) \sin 2\theta_5 \dot{\theta}_6^2 = \gamma_5 \\
&- \left(C_{51} \dot{\theta}_5 + f_{51} \right)
\end{aligned} \tag{5}
$$

$$
\begin{aligned}
&- \left((m_1 + m_2) l_1^2 \theta_2 + m_2 l_1 l_2 \theta_4 \right) \ddot{\theta}_1 + \left((m_1 + m_2) l_1 L S_5 \right. \\
&\left. + m_2 l_1 l_2 \theta_3 + (m_1 + m_2) l_1^2 \theta_1 \right) \ddot{\theta}_2 - \left(m_2 l_1 l_2 \theta_2 \right. \\
&\left. + m_2 l_2^2 \theta_4 \right) \ddot{\theta}_3 + \left(m_2 l_1 l_2 \theta_1 + m_2 l_2^2 \theta_3 + m_2 l_2 L S_5 \right) \ddot{\theta}_4 \\
&- \left((m_1 + m_2) l_1 L \theta_2 C_5 + m_2 l_2 L \theta_4 S_5 \right) \ddot{\theta}_5 \\
&+ \left((m_1 + m_2) L^2 S_5^2 + (m_1 + m_2) l_1^2 \left(\theta_1^2 + \theta_2^2 \right) \right. \\
&\left. + m_2 l_2^2 \left(\theta_3^2 + \theta_4^2 \right) + I_b + I_x S_5 + I_z C_5 + J_6 \right) \ddot{\theta}_6 \\
&+ \left(2 (m_1 + m_2) l_1 L \theta_1 S_5 + 2 m_2 l_2 L \theta_3 S_5 \right. \\
&\left. + 2 m_2 l_1 l_2 (\theta_1 \theta_3 + \theta_2 \theta_4) \right) \ddot{\theta}_6 + \left((m_1 + m_2) l_1 L \theta_2 S_5 \dot{\theta}_5 \right. \\
&\left. + m_2 l_2 L \theta_4 S_5 \dot{\theta}_5 + 2 (m_1 + m_2) l_1 L \theta_1 C_5 \dot{\theta}_6 \right. \\
&\left. + 2 m_2 l_2 L \theta_3 C_5 \dot{\theta}_6 \right) \dot{\theta}_5 \\
&+ \left(2 (m_1 + m_2) l_1^2 \left(\theta_1 \dot{\theta}_1 + \theta_2 \dot{\theta}_2 \right) \right. \\
&\left. + 2 m_2 l_2^2 \left(\theta_3 \dot{\theta}_3 + \theta_4 \dot{\theta}_4 \right) + 2 (m_1 + m_2) l_1 L \dot{\theta}_1 S_5 \right. \\
&\left. + 2 m_2 l_2 L \dot{\theta}_3 S_5 \right) \dot{\theta}_6 \\
&+ \left(2 m_2 l_1 l_2 \left(\theta_4 \dot{\theta}_2 + \theta_2 \dot{\theta}_4 + \theta_3 \dot{\theta}_1 + \theta_1 \dot{\theta}_3 \right) \right) \dot{\theta}_6 \\
&+ \left((m_1 + m_2) L^2 + I_x - I_z \right) \sin 2\theta_5 \dot{\theta}_5 \dot{\theta}_6 = \gamma_6 \\
&- \left(C_{61} \dot{\theta}_6 + f_{61} \right)
\end{aligned} \tag{6}
$$

where M, M_1, m_1, and m_2 are the masses of the boom, the ballast, the hook, and the load, respectively. L, L_1, l_1, and l_2 are the lengths of the boom, the ballast, the rope, and the rigging, respectively. θ_1, θ_3, θ_2, and θ_4 are the components of hook angle and load angle in the vertical and horizontal direction of the boom, respectively. θ_5 and θ_6 are the vertical and horizontal angles of the boom, respectively. In addition, g, J_{k+4}, γ_{k+4}, $C_{(k+4)1}$ and $f_{(k+4)1}$ (k=1,2) are the acceleration of gravity, the moment of inertia for boom motion, the system gains, the boom-driven torque, the viscous friction coefficients, and the static friction or Coulomb friction term. In addition, C_j and S_j ($j = 5, 6$) denote $\cos\theta_j$ and $\sin\theta_j$, respectively. The detailed derivation procedure for (1)-(6) is included in Appendix.

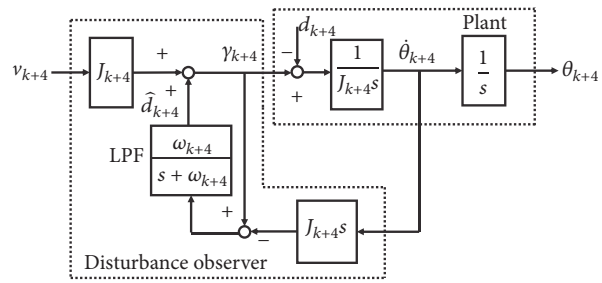

Figure 2: Proposed disturbance observer.

The dynamics of boom-driven systems are [44, 45]

$$
J_{k+4} \ddot{\theta}_{k+4} + d_{k+4} = \gamma_{k+4}, \quad k = 1, 2 \tag{7}
$$

where d_{k+4} denotes the disturbance.

In order to compensate for the above disturbance, the disturbance observer as shown in Figure 2 is designed [43–48]. Then, we have

$$
\ddot{\theta}_{k+4} = v_{k+4} \tag{8}
$$

where v_{k+4} is the control input for vertical and horizontal subsystem, respectively.

Equations (1)-(4) and (8) are represented as follows:

$$
\begin{gathered}
M' \ddot{\Theta}' + K' \Theta' = A_k B' v_{k+4}, \quad k = 1, 2 \\
M' = \begin{bmatrix} 1 & \dfrac{m_2 l_2}{(m_1 + m_2) l_1} \\ \dfrac{l_1}{l_2} & 1 \end{bmatrix}, \\
K' = \begin{bmatrix} \dfrac{g}{l_1} & 0 \\ 0 & \dfrac{g}{l_2} \end{bmatrix}, \\
B' = \begin{bmatrix} \dfrac{1}{l_1} \\ \dfrac{1}{l_2} \end{bmatrix}, \\
\Theta' = \begin{bmatrix} \theta_k \\ \theta_{k+2} \end{bmatrix}
\end{gathered} \tag{9}
$$

where $A_1 = -L \cos\theta_{5f}$ and $A_2 = -L \sin\theta_{5f}$. θ_{5f} is the desired position of the vertical boom angle.

Then, (9) is represented as follows [49]:

$$
\begin{aligned}
M''\ddot{\Psi} + K''\Psi &= A_k B'' v_{k+4}, \quad k = 1, 2 \\
\Psi &= \begin{bmatrix} \psi_k \\ \psi_{k+2} \end{bmatrix} = H^{-1} \begin{bmatrix} \theta_k \\ \theta_{k+2} \end{bmatrix}, \\
H &= \begin{bmatrix} 1 - \dfrac{\omega_k^2 m_1 l_2}{g(m_1 + m_2)} & 1 - \dfrac{\omega_{k+2}^2 m_1 l_2}{g(m_1 + m_2)} \\ 1 & 1 \end{bmatrix} \\
\omega_{k,k+2}^2 &= \left(\frac{(m_1 + m_2)(l_1 + l_2) \mp \sqrt{(l_1 + l_2)^2 (m_1 + m_2)^2 - 4 l_1 l_2 m_1 (m_1 + m_2)}}{2 m_1 l_1 1_2} \right) g,
\end{aligned}
\tag{10}
$$

where $M'' = H^T M' H$, $K'' = H^T K' H$, and $B'' = H^T B'$.

Then, we have

$$
\begin{aligned}
\dot{X} &= A_k' X + A_k b_k v_{k+4}, \quad k = 1, 2 \\
A_k' &= \begin{bmatrix} 0 & 0 & 0 & 1 & 0 & 0 \\ 0 & 0 & 0 & 0 & 1 & 0 \\ 0 & 0 & 0 & 0 & 0 & 1 \\ -\omega_k^2 & 0 & 0 & 0 & 0 & 0 \\ 0 & -\omega_{k+2}^2 & 0 & 0 & 0 & 0 \\ 0 & 0 & 0 & 0 & 0 & 0 \end{bmatrix}, \\
b_k &= \begin{bmatrix} 0 \\ 0 \\ 0 \\ \dfrac{m_1 + m_2}{\delta} \\ -\dfrac{m_1 + m_2}{\delta} \\ 1 \end{bmatrix} \quad X = \begin{bmatrix} \psi_k \\ \psi_{k+2} \\ \theta_{k+4} \\ \dot{\psi}_k \\ \dot{\psi}_{k+2} \\ \dot{\theta}_{k+4} \end{bmatrix}
\end{aligned}
\tag{11}
$$

where $\delta = \sqrt{(l_1 + l_2)^2 (m_1 + m_2)^2 + 2 l_1 l_2 (m_2^2 - m_1^2)}$.

From the above equations, the crane system can be divided into two subsystems (i.e., vertical boom motion and horizontal boom motion subsystems). Therefore, we can design feasible and effective controllers for each subsystem, respectively.

3. Controller Design Process

3.1. Closed-Loop System Representation. The closed-loop control system for rotary crane is

$$
\begin{aligned}
\dot{X} &= \left(A_k' + A_k b_k k_{k+4}^T \right) X, \quad k = 1, 2 \\
k_{k+4}^T &= \left[k_{(k+4)1} \;\; k_{(k+4)2} \;\; k_{(k+4)3} \;\; k_{(k+4)4} \;\; k_{(k+4)5} \;\; k_{(k+4)6} \right]
\end{aligned}
\tag{12}
$$

where $k_{(k+4)1}$, $k_{(k+4)2}$, $k_{(k+4)3}$, $k_{(k+4)4}$, $k_{(k+4)5}$, and $k_{(k+4)6}$ are feedback gains. These gains will be calculated via the LMI-based method in this study.

3.2. Pole Placement Problem by LMI. In linear control theory, if all eigenvalues of matrix $A_k' + A_k b_k k_{k+4}^T$ lie in the left-half of a region shown in Figure 3, the system is stable. Inspired by the literature [43], the following formulations were suggested to solve the pole placement problem in this study:

$$
\begin{aligned}
& A_k' X_1 + X_1 A_k'^T + b_k' M_1 + M_1^T b_k'^T + 2\alpha X_1 < 0 \\
& A_k' X_1 + X_1 A_k'^T + b_k' M_1 + M_1^T b_k'^T + 2\beta X_1 > 0 \\
& \begin{bmatrix} \sin\varphi \left(A_k' X_1 + X_1 A_k'^T + b_k' M_1 + M_1^T b_k'^T \right) & \cos\varphi \left(A_k' X_1 - X_1 A_k'^T + b_k' M_1 - M_1^T b_k'^T \right) \\ \cos\varphi \left(-A_k' X_1 + X_1 A_k'^T - b_k' M_1 + M_1^T b_k'^T \right) & \sin\varphi \left(A_k' X_1 + X_1 A_k'^T + b_k' M_1 + M_1^T b_k'^T \right) \end{bmatrix} < 0 \\
& X_1 > 0
\end{aligned}
\tag{13}
$$

where $M_1 = k_{k+4}^T X_1$ and $b_k' = A_k b_k$.

3.3. Optimal Regulator Problem by LMI. This subsection proposes an LQR method to achieve the optimal control problem. Hence, the following cost function J is considered [43]:

$$J = \frac{1}{2}\int_0^{\infty} \left(Q_{k+4}^{1/2}X_2 + R_{k+4}^{1/2}v_{k+4}\right)^T \cdot \left(Q_{k+4}^{1/2}X_2 + R_{k+4}^{1/2}v_{k+4}\right) dt \tag{14}$$

where $Q_{k+4} \geq 0$ and $R_{k+4} > 0$.

Then, inspired by the method presented in [50], the above problem can be converted into the problem of finding X_2, Y, and k_i such that Trace(Y) is minimal with the following constraints:

$$\begin{gathered}
\begin{bmatrix} \left(A_k'X_2 + b_k'M_2\right) + \left(X_2A_k'^T + M_2^Tb_k'^T\right) & 0 \\ 0 & -I \end{bmatrix} < 0 \\
\begin{bmatrix} Y & \left(Q_{k+4}^{1/2}X_2 + R_{k+4}^{1/2}M_2\right) \\ \left(Q_{k+4}^{1/2}X_2 + R_{k+4}^{1/2}M_2\right)^T & X_2 \end{bmatrix} > 0
\end{gathered} \tag{15}$$

where $M_2 = k_{k+4}^T X_2$.

3.4. Controller Design. In this study, we synthesize the above two problems to obtain the controller by setting $X_1 = X_2$ and $M_1 = M_2$ [43]:

$$\begin{gathered}
A_k'X_1 + X_1A_k'^T + b_k'M_1 + M_1^Tb_k'^T + 2\alpha X_1 < 0 \\
A_k'X_1 + X_1A_k'^T + b_k'M_1 + M_1^Tb_k'^T + 2\beta X_1 > 0 \\
\begin{bmatrix} \sin\varphi\left(A_k'X_1 + X_1A_k'^T + b_k'M_1 + M_1^Tb_k'^T\right) & \cos\varphi\left(A_k'X_1 - X_1A_k'^T + b_k'M_1 - M_1^Tb_k'^T\right) \\ \cos\varphi\left(-A_k'X_1 + X_1A_k'^T - b_k'M_1 + M_1^Tb_k'^T\right) & \sin\varphi\left(A_k'X_1 + X_1A_k'^T + b_k'M_1 + M_1^Tb_k'^T\right) \end{bmatrix} < 0 \\
\begin{bmatrix} Y & \left(Q_{k+4}^{1/2}X_2 + R_{k+4}^{1/2}M_2\right) \\ \left(Q_{k+4}^{1/2}X_2 + R_{k+4}^{1/2}M_2\right)^T & X_1 \end{bmatrix} > 0
\end{gathered} \tag{16}$$

4. Results and Discussion

4.1. Simulation Conditions. In order to evaluate the control performance of the proposed controller, a cycloid-like motion trajectory was applied to the crane system [43]:

$$\theta_{(k+4)d} = \begin{cases} \left(\theta_{(k+4)f} - \theta_{(k+4)0}\right)\left\{\dfrac{t}{t_s} - \dfrac{1}{2\pi}\sin\left(2\pi\dfrac{t}{t_s}\right)\right\} + x_{(k+4)0} & t \in [0, t_s) \\ \theta_{(k+4)f} & t \in \left(t_s, t_f\right] \end{cases} \tag{17}$$

where $\theta_{(k+4)f}$, $x_{(k+4)0}$, t_r, and t_f are the desired boom angle, the initial boom angle, the reaching time, and the finish time. These parameters were selected as $\theta_{50} = 0$[deg], $\theta_{60} = 0$[deg], $\theta_{5f} = 30$[deg], $\theta_{6f} = 45$[deg], $t_r = 3$[s], and $t_f = 10$[s].

Parameters as shown in Figure 3 were selected as 80, 1, and 30, respectively. We also set $Q_5 = \text{diag}\{150, 15, 50, 315, 15, 50\}$, $Q_6 = \text{diag}\{50, 150, 50, 300, 150, 50\}$, and $R_5 = R_6 = 1$ in (16). The controller gains for the decoupled linear system were obtained as follows by the method proposed in Section 3 with the rotary crane parameters shown in Table 1, when the rope length varies from 0.25[m] to from 0.75[m].

$$k_5^T = \begin{bmatrix} -39.65 & 124.08 & 10.61 & -17.12 & -8.75 & 14.73 \end{bmatrix} \tag{18}$$

$$k_6^T = \begin{bmatrix} -61.92 & 210.78 & 10.77 & -27.01 & -12.99 & 14.45 \end{bmatrix} \tag{19}$$

Using the relationship shown in (10), the gains for the original rotary crane are

$$k_5'^T = \begin{bmatrix} 103.08 & -17.82 & 10.61 & 137.15 & -3.11 & 14.73 \end{bmatrix} \tag{20}$$

$$k_6'^T = \begin{bmatrix} 177.99 & -27.30 & 10.77 & 231.19 & -4.10 & 14.45 \end{bmatrix} \tag{21}$$

4.2. Stability Analysis. We conducted several numerical to explain the robust stability of the proposed control system when the rope length l_1 varies from 0.25[m] to from 0.75[m]. The initial poles of the vertical boom motion subsystem were set to $p_{11} = -1.04$[1/s], $p_{21} = -1.45 + 9.07j$[1/s], $p_{31} = -1.45 - 9.07j$[1/s], $p_{41} = -4.80 + 6.92j$[1/s], $p_{51} = -4.80 - 6.92j$[1/s], and $p_{61} = -6.07$[1/s], and the initial poles of the horizontal boom motion subsystem were set to $p_{12} = -1.51 + 9.54j$[1/s], $p_{22} = -1.51 - 9.45j$[1/s], $p_{32} = -4.96 + 6.30j$[1/s], $p_{42} = -4.96 - 6.30j$[1/s], $p_{52} = -7.62 + 2.64j$[1/s], and $p_{62} = -7.62 - 2.64j$[1/s]. It is confirmed that the crane system can be stabilized by the controller from the simulation results in Figure 4.

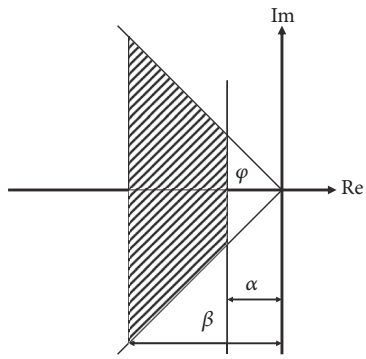

Figure 3: Stable region.

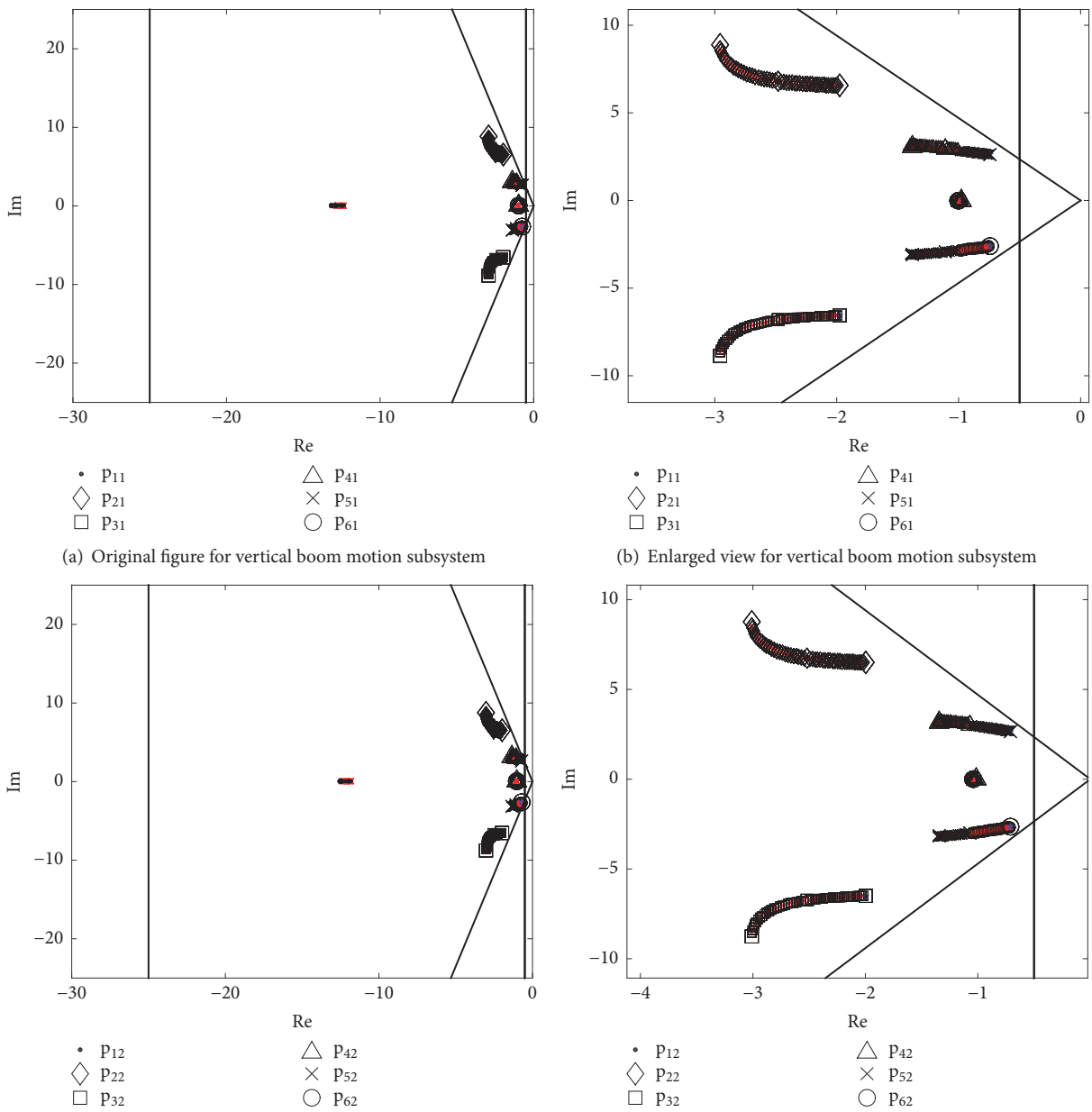

(a) Original figure for vertical boom motion subsystem

(b) Enlarged view for vertical boom motion subsystem

(c) Original figure for horizontal boom motion subsystem

(d) Enlarged view for horizontal boom motion subsystem

Figure 4: Poles placement.

Table 1: Rotary crane model.

M_0[kg]	0.86	M_1[kg]	2.03	m_1[kg]	2.00
m_2[kg]	0.56	L[m]	0.65	L_1[m]	0.19
l_1[m]	0.50	l_2[m]	0.30	g[m/s^2]	9.80
J_5[kgm^2]	0.56	J_6[kgm^2]	0.65	I_b[Nm]	0.38
C_{51}[Nm/(rad/s)]	1.57	C_{61}[Nm/(rad/s)]	1.39	f_{51}[Nm]	3.91
f_{61}[Nm]	3.58	–	–	–	–

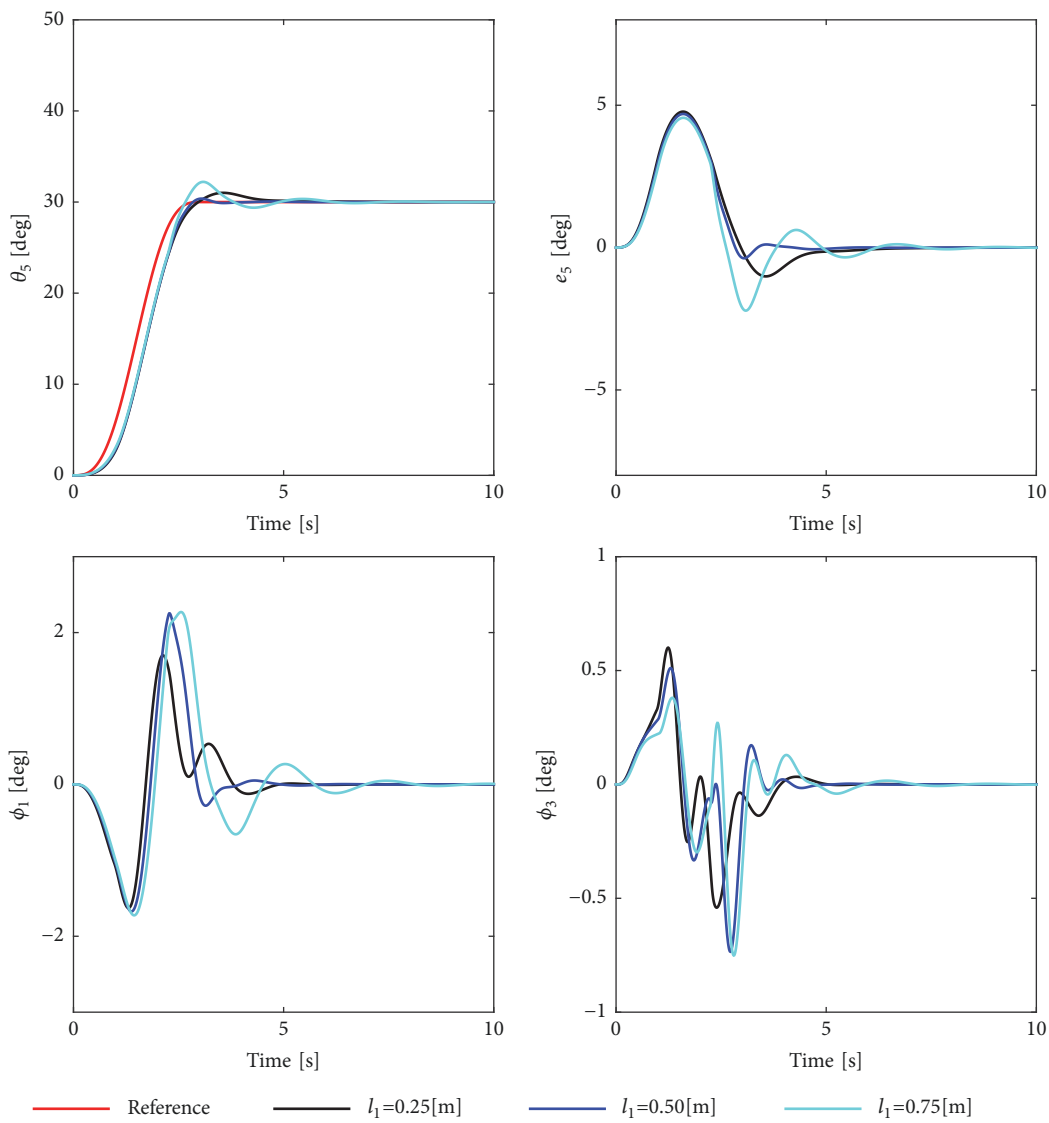

Figure 5: Simulations under the decoupled linear crane model in vertical boom motion subsystem.

4.3. Simulation Results. We conducted several simulations based on the linear model under different rope length, firstly. The results for the vertical subsystem are shown in Figure 5. Although there are transient errors and slight overshoot in these figures, the vertical boom motion converges to the desired position rapidly. Meanwhile, there is almost no residual modal swaying vibration. On the other hand, the results for the horizontal subsystem are shown in Figure 6. Almost the same results were obtained as those in Figure 5. The results based on the original crane system for the terms of the load sways θ_1, θ_2, θ_3, θ_4, the tracking error for vertical boom angle e_5, the tracking errors for horizontal boom angle e_6, the vertical boom angle θ_5, the horizontal boom angle θ_6, and the control inputs v_5 and v_6 are shown in Figure 7. Because of the effect of the ignored nonlinearity of the crane model, the residual

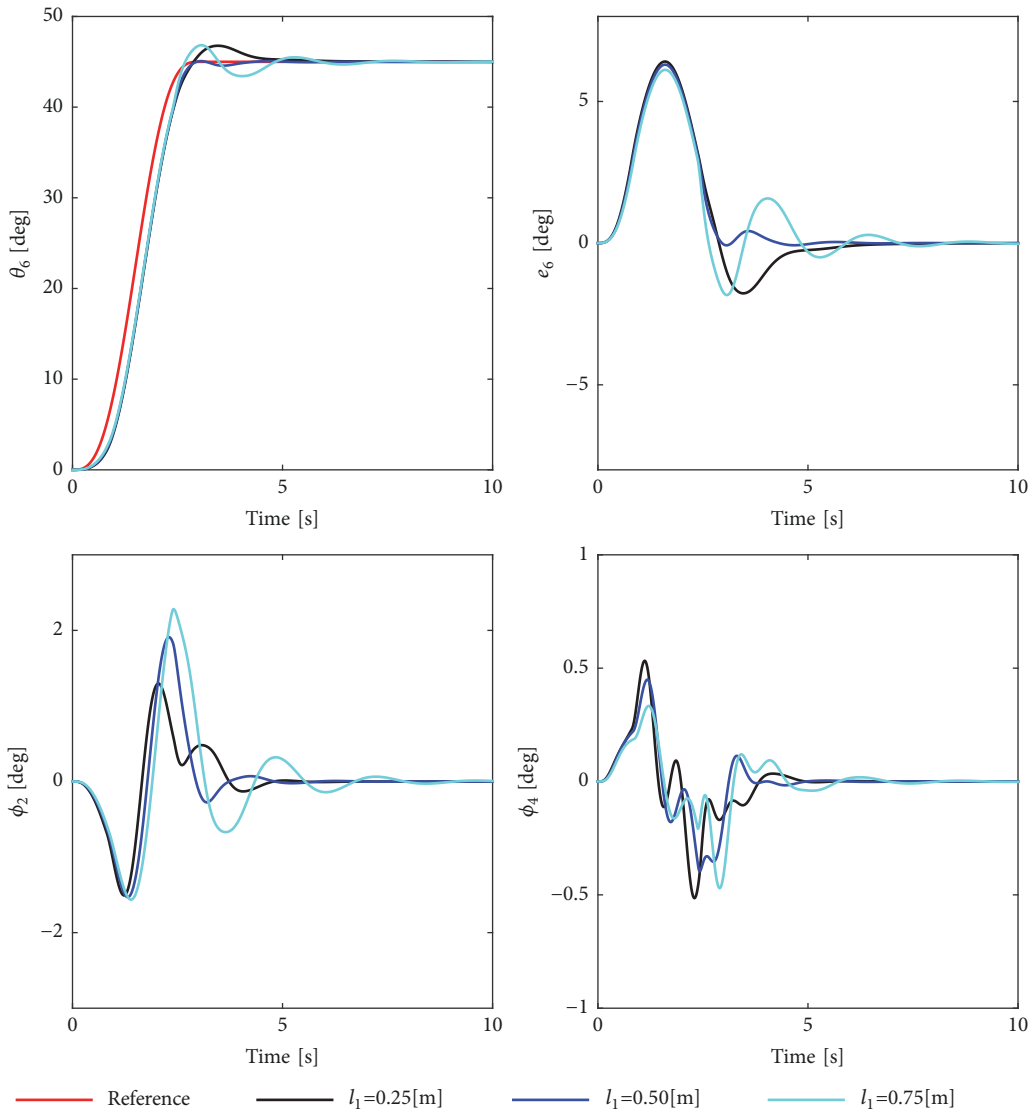

Figure 6: Simulations under the decoupled linear crane model in horizontal boom motion subsystem.

swaying angles are bigger than those in Figures 5 and 6.

For verifying that the presented controller also has robustness to the rigging length variation, we conducted simulations with the gains in (20) and (21) by set the l_2 as $l_2 = 0.20[\mathrm{m}]$ and $l_2 = 0.40[\mathrm{m}]$. By comparing the results in Figures 7 and 8, it is found that although the second sway angle of the horizontal direction θ_4 increases with the increase of the rigging length, it still remains in a reasonable range.

4.4. Comparative Simulation. In order to confirm the proposed method can provide superior robust performance, some comparative simulations were conducted by a conventional state feedback controller. A dominant poles placement method was applied to calculate the controller gains which are as follows:

$$k_5''^T = \begin{bmatrix} -253.27 & 6.42 & 11.12 & -292.64 & -41.28 & -47.10 \end{bmatrix} \tag{22}$$

$$k_6''^T = \begin{bmatrix} -460.06 & 14.78 & 19.26 & -499.43 & -62.48 & -81.58 \end{bmatrix} \tag{23}$$

The results are shown in Figure 9. Although the load sway angles reduced completely under condition $l_1 = 0.25[\mathrm{m}]$ or $l_1 = 0.50[\mathrm{m}]$, the load sway angles cannot be reduced by using gains in (22) and (23) under condition $l_1 = 0.75[\mathrm{m}]$. Meanwhile, the quantitative analyses between the proposed method and the existing one are in Tables 2–4. It is indicated that the presented method can furnish preferable robust performance than the traditional one from these figures and tables.

5. Conclusion

In order to achieve the robust control for a rotary crane with double-pendulum effect, a simple model for controller design is obtained by linearizing and decoupling the complex

Table 2: Quantified results under condition $l_1 = 0.25$[m].

Control method	The maximum value of tracking error e_{5max}[deg]	The maximum value of tracking error e_{6max}[deg]
Proposed controller	3.25	3.84
Conventional controller	3.08	3.84
	The maximum value of hook sway angle θ_{1max}[deg]	The maximum value of hook sway angle θ_{2max}[deg]
Proposed controller	2.20	1.70
Conventional controller	1.92	1.82
	The maximum value of load sway angle θ_{3max}[deg]	The maximum value of load sway angle θ_{4max}[deg]
Proposed controller	2.49	2.14
Conventional controller	2.61	2.56

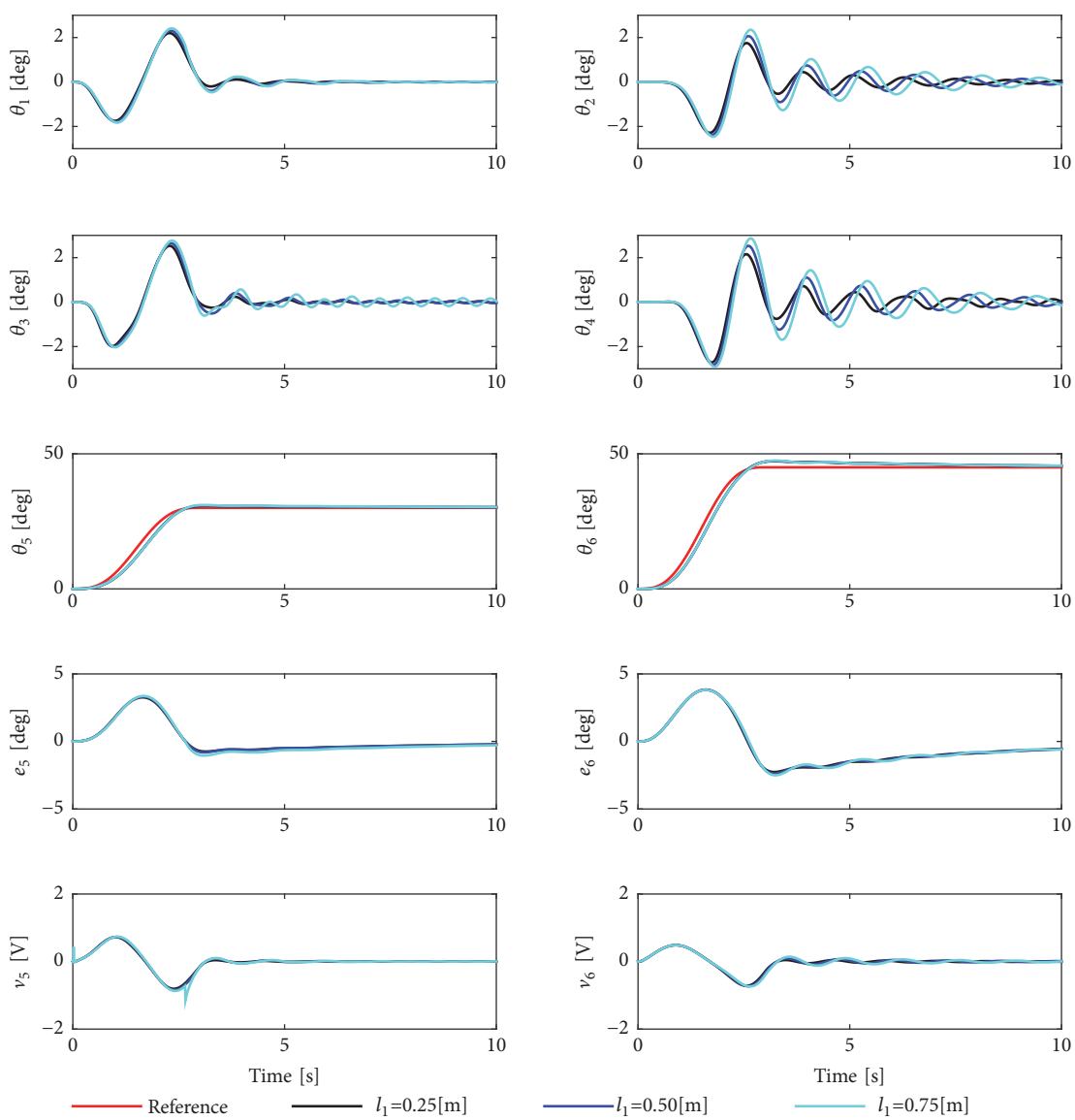

Figure 7: Simulations under the original crane model with different rope length.

Table 3: Quantified results under condition $l_1 = 0.50$[m].

Control method	The maximum value of tracking error e_{5max}[deg]	The maximum value of tracking error e_{6max}[deg]
Proposed controller	3.31	3.82
Conventional controller	3.12	3.82
	The maximum value of hook sway angle θ_{1max}[deg]	The maximum value of hook sway angle θ_{2max}[deg]
Proposed controller	2.31	2.01
Conventional controller	2.10	2.10
	The maximum value of load sway angle θ_{3max}[deg]	The maximum value of load sway angle θ_{4max}[deg]
Proposed controller	2.64	2.53
Conventional controller	2.75	2.94

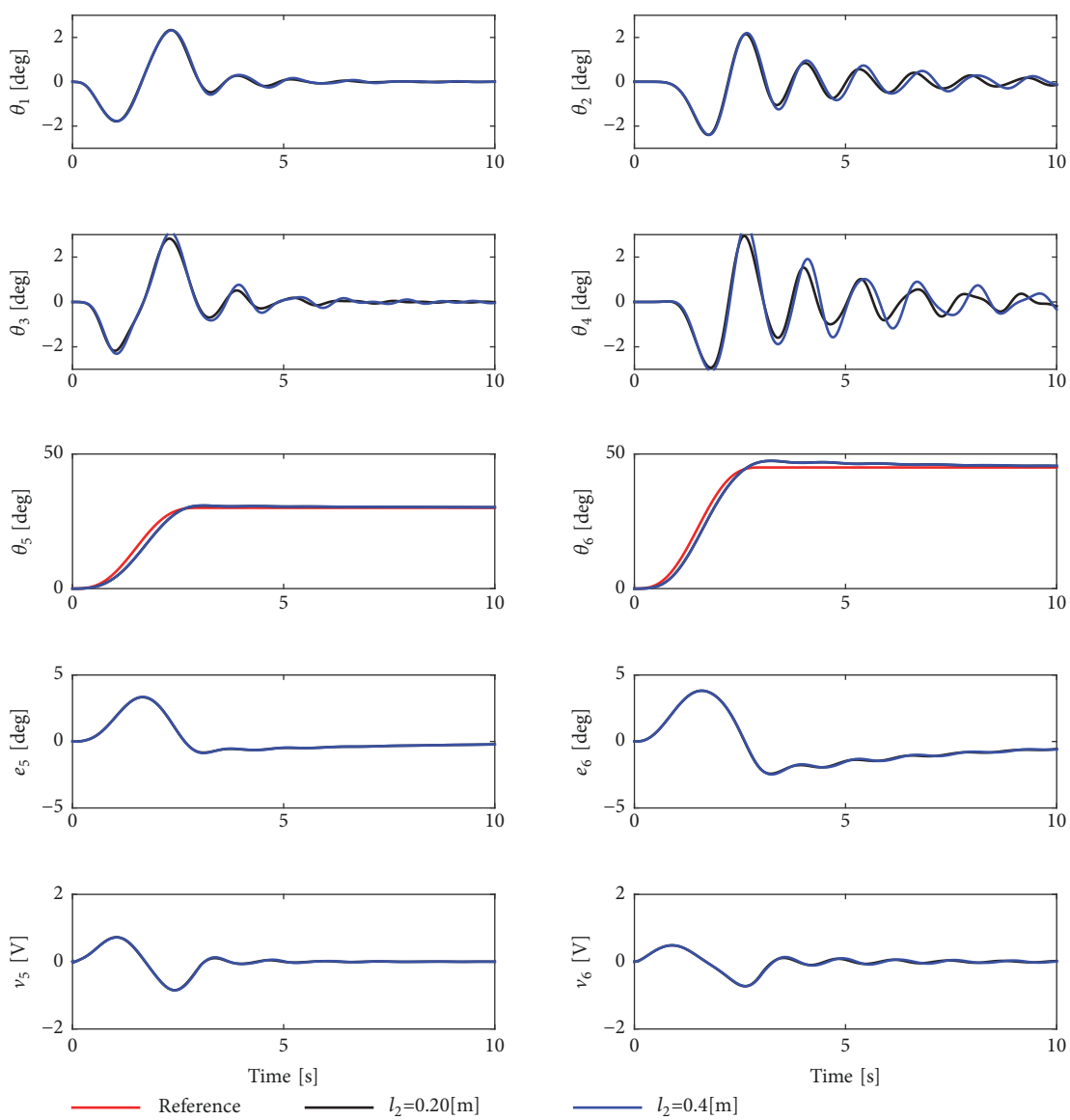

Figure 8: Simulations under the original crane model with different rigging length.

Table 4: Quantified results under condition $l_1 = 0.75$[m].

Control method	The maximum value of tracking error e_{5max}[deg]	The maximum value of tracking error e_{6max}[deg]
Proposed controller	3.36	3.81
Conventional controller	3.10	3.75
	The maximum value of hook sway angle θ_{1max}[deg]	The maximum value of hook sway angle θ_{2max}[deg]
Proposed controller	2.40	2.31
Conventional controller	3.01	3.00
	The maximum value of load sway angle θ_{3max}[deg]	The maximum value of load sway angle θ_{4max}[deg]
Proposed controller	2.76	2.81
Conventional controller	4.21	5.14

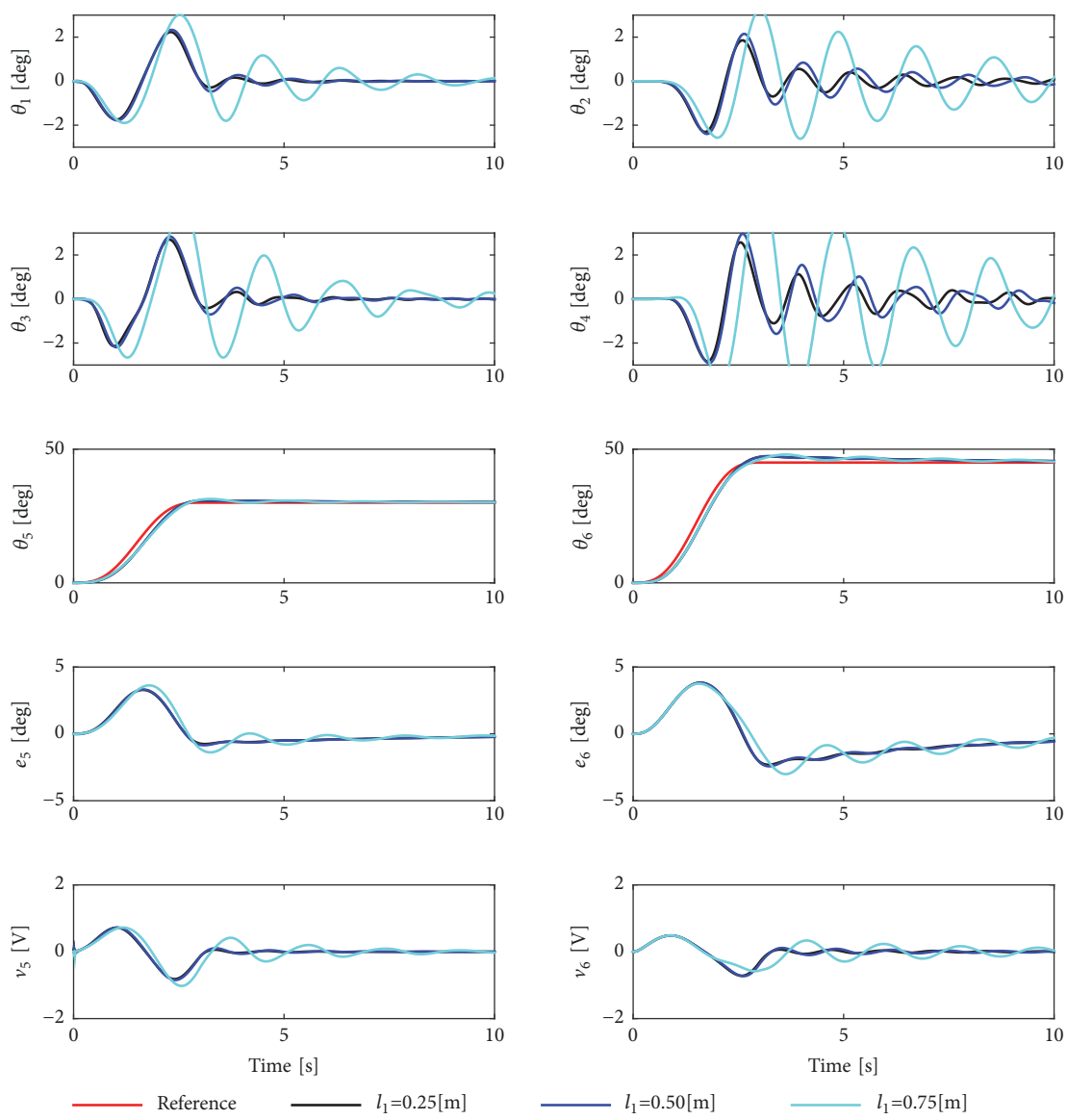

Figure 9: Conventional controller results.

nonlinear model of rotary crane. Then, a linear feedback controller which can furnish robust performance was presented. Finally, numerical simulations verified the effectiveness of the proposed method by comparing with a traditional approach.

Appendix

This section presents the derivation of the crane dynamics in (1)-(6). From Figure 1, the position of the hook with respect to the origin of coordinates is presented as follows:

$$\begin{aligned} x_1 &= (L\sin\theta_5 + l_1\theta_1)\cos\theta_6 - l_1\theta_2\sin\theta_6 \\ y_1 &= (L\sin\theta_5 + l_1\theta_1)\sin\theta_6 + l_1\theta_2\cos\theta_6 \\ z_1 &= L\cos\theta_5 - l_1\cos\sqrt{\theta_1^2+\theta_2^2} \end{aligned} \tag{A.1}$$

Then, the position of the load with respect to the origin of coordinates is

$$\begin{aligned} x_2 &= (L\sin\theta_5 + l_1\theta_1 + l_2\theta_3)\cos\theta_6 \\ &\quad - (l_1\theta_2 + l_2\theta_4)\sin\theta_6 \\ y_2 &= (L\sin\theta_5 + l_1\theta_1 + l_2\theta_3)\sin\theta_6 \\ &\quad - (l_1\theta_2 + l_2\theta_4)\cos\theta_6 \\ z_2 &= L\cos\theta_5 - l_1\cos\sqrt{\theta_1^2+\theta_2^2} - l_2\cos\sqrt{\theta_3^2+\theta_4^2} \end{aligned} \tag{A.2}$$

Taking the time derivation of (A.1) and (A.2), we have

$$\begin{aligned} \dot{x}_1 &= L\dot{\theta}_5\cos\theta_5\cos\theta_6 - L\dot{\theta}_6\sin\theta_5\sin\theta_6 \\ &\quad + l_1\dot{\theta}_1\cos\theta_6 - l_1\theta_1\dot{\theta}_6\sin\theta_6 - l_1\dot{\theta}_2\sin\theta_6 \\ &\quad - l_1\theta_2\dot{\theta}_6\cos\theta_6 \\ \dot{y}_1 &= L\dot{\theta}_5\cos\theta_5\sin\theta_6 - L\dot{\theta}_6\sin\theta_5\cos\theta_6 \\ &\quad + l_1\dot{\theta}_1\sin\theta_6 + l_1\theta_1\dot{\theta}_6\cos\theta_6 + l_1\dot{\theta}_2\cos\theta_6 \\ &\quad - l_1\theta_2\dot{\theta}_6\sin\theta_6 \\ \dot{z}_1 &= -L\dot{\theta}_5\sin\theta_5 + l_1\left(\theta_1\dot{\theta}_1 + \theta_2\dot{\theta}_2\right) \end{aligned} \tag{A.3}$$

and

$$\begin{aligned} \dot{x}_2 &= L\dot{\theta}_5\cos\theta_5\cos\theta_6 - L\dot{\theta}_6\sin\theta_5\sin\theta_6 \\ &\quad + l_1\dot{\theta}_1\cos\theta_6 - l_1\theta_1\dot{\theta}_6\sin\theta_6 - l_1\dot{\theta}_2\sin\theta_6 \\ &\quad - l_1\theta_2\dot{\theta}_6\cos\theta_6 \\ &= +l_2\dot{\theta}_3\cos\theta_6 - l_2\theta_3\dot{\theta}_6\sin\theta_6 - l_2\dot{\theta}_4\sin\theta_6 \\ &\quad - l_2\theta_4\dot{\theta}_6\cos\theta_6 \\ \dot{y}_2 &= L\dot{\theta}_5\cos\theta_5\sin\theta_6 - L\dot{\theta}_6\sin\theta_5\cos\theta_6 \\ &\quad + l_1\dot{\theta}_1\sin\theta_6 + l_1\theta_1\dot{\theta}_6\cos\theta_6 + l_1\dot{\theta}_2\cos\theta_6 \\ &\quad - l_1\theta_2\dot{\theta}_6\sin\theta_6 \\ &= +l_2\dot{\theta}_3\sin\theta_6 - l_2\theta_3\dot{\theta}_6\cos\theta_6 + l_2\dot{\theta}_4\cos\theta_6 \\ &\quad - l_2\theta_4\dot{\theta}_6\sin\theta_6 \\ \dot{z}_2 &= -L\dot{\theta}_5\sin\theta_5 + l_1\left(\theta_1\dot{\theta}_1 + \theta_2\dot{\theta}_2\right) \\ &\quad + l_2\left(\theta_3\dot{\theta}_3 + \theta_4\dot{\theta}_4\right) \end{aligned} \tag{A.4}$$

Hence, the kinetic energy of the hook and the load T_1 is as follows:

$$\begin{aligned} T_1 &= \frac{1}{2}m_1\left(\dot{x}_1^2 + \dot{y}_1^2 + \dot{z}_1^2\right) + \frac{1}{2}m_2\left(\dot{x}_2^2 + \dot{y}_2^2 + \dot{z}_2^2\right) \\ &= \frac{1}{2}m_1L^2\dot{\theta}_5^2 + \frac{1}{2}m_1l_1^2\dot{\theta}_1^2 + m_2l_1^2\theta_1\dot{\theta}_6\dot{\theta}_2 \\ &\quad + m_2l_1l_2\dot{\theta}_2\dot{\theta}_4 - m_2l_2^2\dot{\theta}_3\theta_4\dot{\theta}_6 + m_2l_2^2\theta_3\dot{\theta}_6\dot{\theta}_4 \\ &\quad - m_2l_1^2\dot{\theta}_1\theta_2\dot{\theta}_6 + m_2l_1l_2\dot{\theta}_1\dot{\theta}_3 \\ &\quad - m_2Ll_1\dot{\theta}_5\cos\theta_5\theta_2\dot{\theta}_6 - m_2Ll_2\dot{\theta}_5\cos\theta_5\theta_4\dot{\theta}_6 \\ &\quad + \frac{1}{2}m_2l_2^2\dot{\theta}_3^2 + \frac{1}{2}m_2l_1^2\dot{\theta}_1^2 + \frac{1}{2}m_2l_1^2\dot{\theta}_2^2 + \frac{1}{2}m_2L^2\dot{\theta}_6^2 \\ &\quad + \frac{1}{2}m_2l_2^2\dot{\theta}_4^2 + \frac{1}{2}m_2L^2\dot{\theta}_5^2 + \frac{1}{2}m_2l_2^2\theta_4^2\dot{\theta}_6^2 \\ &\quad + \frac{1}{2}m_2l_1^2\theta_1^2\dot{\theta}_6^2 + \frac{1}{2}m_2l_1^2\theta_2^2\dot{\theta}_6^2 + \frac{1}{2}m_2l_2^2\theta_3^2\dot{\theta}_6^2 \\ &\quad + m_2Ll_2\dot{\theta}_5\cos\theta_5\dot{\theta}_3 + m_2L\dot{\theta}_6^2\sin\theta_5l_1\theta_1 \\ &\quad + m_2L\dot{\theta}_6\sin\theta_5l_1\dot{\theta}_2 + m_2L\dot{\theta}_6^2\sin\theta_5l_2\theta_3 \\ &\quad + m_2L\dot{\theta}_6\sin\theta_5l_2\dot{\theta}_4 - m_2l_1\dot{\theta}_1l_2\theta_4\dot{\theta}_6 \\ &\quad + m_2l_1\theta_1\dot{\theta}_6^2l_2\theta_3 + m_2l_1\theta_1\dot{\theta}_6l_2\dot{\theta}_4 + m_2l_1\dot{\theta}_2l_2\theta_3\dot{\theta}_6 \\ &\quad - m_2l_1\theta_2\dot{\theta}_6l_2\dot{\theta}_3 + m_2L\theta_5\cos\theta_5l_1\dot{\theta}_1 \\ &\quad + m_2l_1\theta_2\dot{\theta}_6^2l_2\theta_4 - \frac{1}{2}m_2L^2\dot{\theta}_6^2\cos^2\theta_5 \\ &\quad + \frac{1}{2}m_1l_1^2\left(\theta_1^2\dot{\theta}_1^2 + \theta_2^2\dot{\theta}_2^2\right) \\ &\quad - m_1L\dot{\theta}_5\sin\theta_5l_1\left(\theta_1\dot{\theta}_1 + \theta_2\dot{\theta}_2\right) \\ &\quad + m_1l_1^2\theta_1\dot{\theta}_1\theta_2\dot{\theta}_2 + \frac{1}{2}m_1l_1^2\dot{\theta}_2^2 \\ &\quad + \frac{1}{2}m_1l_1^2\dot{\theta}_6^2\left(\theta_1^2 + \theta_2^2\right) + m_1L\dot{\theta}_5\cos\theta_5l_1\dot{\theta}_1 \\ &\quad + m_1L\dot{\theta}_6^2\sin\theta_5l_1\theta_1 + m_1L\dot{\theta}_6\sin\theta_5l_1\dot{\theta}_2 \end{aligned}$$

$$
\begin{aligned}
&+ m_1 l_1^2 \theta_1 \dot{\theta}_6 \dot{\theta}_2 - m_1 L \dot{\theta}_5 \cos\theta_5 l_1 \theta_2 \dot{\theta}_6 \\
&- m_1 l_1^2 \dot{\theta}_1 \theta_2 \dot{\theta}_6 - \frac{1}{2} m_1 L^2 \dot{\theta}_6^2 \cos^2\theta_5 \\
&+ \frac{1}{2} m_2 l_2^2 \left(\theta_3^2 \dot{\theta}_3^2 + \theta_4^2 \dot{\theta}_4^2\right) \\
&+ \frac{1}{2} m_2 l_1^2 \left(\theta_1^2 \dot{\theta}_1^2 + \theta_2^2 \dot{\theta}_2^2\right) + m_2 l_1^2 \theta_1 \dot{\theta}_1 \theta_2 \dot{\theta}_2 \\
&+ m_2 l_2^2 \theta_3 \dot{\theta}_3 \theta_4 \dot{\theta}_4 \\
&- m_2 L \dot{\theta}_5 \sin\theta_5 l_1 \left(\theta_1 \dot{\theta}_1 + \theta_2 \dot{\theta}_2\right) \\
&- m_2 L \dot{\theta}_5 \sin\theta_5 l_2 \left(\theta_3 \dot{\theta}_3 + \theta_4 \dot{\theta}_4\right) \\
&+ m_2 l_1 \theta_1 \dot{\theta}_1 l_2 \left(\theta_3 \dot{\theta}_3 + \theta_4 \dot{\theta}_4\right) \\
&+ m_2 l_1 \theta_2 \dot{\theta}_2 l_2 \left(\theta_3 \dot{\theta}_3 + \theta_4 \dot{\theta}_4\right) + \frac{1}{2} m_1 L^2 \dot{\theta}_6^2
\end{aligned}
\tag{A.5}
$$

Next, the kinetic energy of the boom T_2 and the ballast T_3 can be presented as follows:

$$T_2 = \frac{1}{2}\left(I_x \dot{\theta}_6^2 \sin^2\theta_5 + I_y \dot{\theta}_5^2 + I_z \dot{\theta}_6^2 \cos^2\theta_5\right) \tag{A.6}$$

$$T_3 = \frac{1}{2} I_b \dot{\theta}_6^2 \tag{A.7}$$

where I_x, I_y, and I_z are the moment inertia of the boom in 3D space; I_b is the moment inertia of the ballast. The total kinetic energy of the crane system is

$$T = T_1 + T_2 + T_3 \tag{A.8}$$

The potential energy of the hook and load U_1, the boom U_2, and the ballast U_3 can be presented as follows, respectively:

$$
\begin{aligned}
U_1 &= m_1 g \left(L\cos\theta_5 - l_1 \cos\sqrt{\theta_1^2 + \theta_2^2}\right) \\
&\quad + m_2 g \left(L\cos\theta_5 - l_1 \cos\sqrt{\theta_1^2 + \theta_2^2}\right. \\
&\quad \left. - l_2 \cos\sqrt{\theta_3^2 + \theta_4^2}\right) \\
U_2 &= \frac{1}{2} M g L \cos\theta_5 \\
U_3 &= -\frac{1}{2} M_1 g L_1 \cos\theta_5
\end{aligned}
\tag{A.9}
$$

Hence, the total potential energy of the rotary crane is

$$
\begin{aligned}
U &= U_1 + U_2 + U_3 \\
&= g\left(\frac{1}{2} M L + (m_1 + m_2) L - \frac{1}{2} M_1 L_1\right) \cos\theta_5 \\
&\quad - (m_1 + m_2) g l_1 \cos\sqrt{\theta_1^2 + \theta_2^2} \\
&\quad - m_2 g l_2 \cos\sqrt{\theta_3^2 + \theta_4^2}
\end{aligned}
\tag{A.10}
$$

where g is the gravitational acceleration.

Lagrange's function L is presented as the difference between the kinetic energy T and the potential energy U.

$$L = T - U \tag{A.11}$$

Then, the double-pendulum rotary crane model can be derived by using Lagrange's equations of motion.

Data Availability

The data used to support the findings of this study are included within the article.

Conflicts of Interest

The authors declare that there are no conflicts of interest regarding the publication of this article.

Acknowledgments

This work is supported in part by the National Natural Science Foundation of China under Grant 61703202 and in part by the Key Research Development Project of Jiangsu Province under Grant BE2017164.

References

[1] L. Ramli, Z. Mohamed, A. M. Abdullahi, H. Jaafar, and I. M. Lazim, "Control strategies for crane systems: A comprehensive review," *Mechanical Systems and Signal Processing*, vol. 95, pp. 1–23, 2017.

[2] X. Xie, J. Huang, and Z. Liang, "Using continuous function to generate shaped command for vibration reduction," *Proceedings of the Institution of Mechanical Engineers, Part I: Journal of Systems and Control Engineering*, vol. 227, no. 6, pp. 523–528, 2013.

[3] J. Huang, E. Maleki, and W. Singhose, "Dynamics and swing control of mobile boom cranes subject to wind disturbances," *IET Control Theory & Applications*, vol. 7, no. 9, pp. 1187–1195, 2013.

[4] H. Saeidi, M. Naraghi, and A. A. Raie, "A neural network self tuner based on input shapers behavior for anti sway system of gantry cranes," *Journal of Vibration and Control*, vol. 19, no. 13, pp. 1936–1949, 2013.

[5] W. Singhose and J. Vaughan, "Reducing vibration by digital filtering and input shaping," *IEEE Transactions on Control Systems Technology*, vol. 19, no. 6, pp. 1410–1420, 2011.

[6] W. Singhose, R. Eloundou, and J. Lawrence, "Command generation for flexible systems by input shaping and command smoothing," *Journal of Guidance, Control, and Dynamics*, vol. 33, no. 6, pp. 1697–1707, 2010.

[7] M. J. Maghsoudi, Z. Mohamed, A. R. Husain, and M. O. Tokhi, "An optimal performance control scheme for a 3D crane," *Mechanical Systems and Signal Processing*, vol. 66-67, pp. 756–768, 2016.

[8] N. Sun and Y. Fang, "An efficient online trajectory generating method for underactuated crane systems," *International Journal of Robust and Nonlinear Control*, vol. 24, no. 11, pp. 1653–1663, 2014.

[9] X. Zhang, Y. Fang, and N. Sun, "Minimum-time trajectory planning for underactuated overhead crane systems with state and

control constraints," *IEEE Transactions on Industrial Electronics*, vol. 61, no. 12, pp. 6915–6925, 2014.

[10] L. A. Tuan, S.-G. Lee, D. H. Ko, and L. C. Nho, "Combined control with sliding mode and partial feedback linearization for 3D overhead cranes," *International Journal of Robust and Nonlinear Control*, vol. 24, no. 18, pp. 3372–3386, 2014.

[11] Q. H. Ngo and K.-S. Hong, "Sliding-mode antisway control of an offshore container crane," *IEEE/ASME Transactions on Mechatronics*, vol. 17, no. 2, pp. 201–209, 2012.

[12] C. Li, Z. Ding, J. Yi, Y. Lv, and G. Zhang, "Deep belief network based hybrid model for building energy consumption prediction," *Energies*, vol. 11, no. 1, p. 242, 2018.

[13] C. Li, J. Yi, H. Wang, G. Zhang, and J. Li, "Interval data driven construction of shadowed sets with application to linguistic word modelling," *Information Sciences*, 2018.

[14] D. Qian, C. Li, S. Lee, and C. Ma, "Robust formation maneuvers through sliding mode for multi-agent systems with uncertainties," *IEEE/CAA Journal of Automatica Sinica*, vol. 5, no. 1, pp. 342–351, 2018.

[15] D. Qian, S. Tong, J. Guo, and S. Lee, "Leader-follower-based formation control of nonholonomic mobile robots with mismatched uncertainties via integral sliding mode," *Proceedings of the Institution of Mechanical Engineers, Part I: Journal of Systems and Control Engineering*, vol. 229, no. 6, pp. 559–569, 2015.

[16] D. Qian, S. Tong, H. Liu, and X. Liu, "Load frequency control by neural-network-based integral sliding mode for nonlinear power systems with wind turbines," *Neurocomputing*, vol. 173, pp. 875–885, 2016.

[17] N. Sun, Y. Fang, H. Chen, and B. He, "Adaptive nonlinear crane control with load hoisting/lowering and unknown parameters: Design and experiments," *IEEE/ASME Transactions on Mechatronics*, vol. 20, no. 5, pp. 2107–2119, 2015.

[18] J. Smoczek and J. Szpytko, "Particle swarm optimization-based multivariable generalized predictive control for an overhead crane," *IEEE/ASME Transactions on Mechatronics*, vol. 22, no. 1, pp. 258–268, 2017.

[19] D. Jolevski and O. Bego, "Model predictive control of gantry/bridge crane with anti-sway algorithm," *Journal of Mechanical Science and Technology*, vol. 29, no. 2, pp. 827–834, 2015.

[20] N. Sun, Y. Fang, H. Chen, Y. Fu, and B. Lu, "Nonlinear stabilizing control for ship-mounted cranes with ship roll and heave movements: design, analysis, and experiments," *IEEE Transactions on Systems, Man, and Cybernetics: Systems*, vol. 48, no. 10, pp. 1781–1793, 2018.

[21] N. Sun, T. Yang, H. Chen, Y. Fang, and Y. Qian, "Adaptive anti-swing and positioning control for 4-DOF rotary cranes subject to uncertain/unknown parameters with hardware experiments," *IEEE Transactions on Systems, Man, and Cybernetics: Systems*, pp. 1–13, 2017.

[22] X. Wu and X. He, "Control of the bridge crane by constructing a Lyapunov function: theoretical design and experimental verification," *Transactions of the Institute of Measurement and Control*, vol. 39, no. 12, pp. 1763–1770, 2017.

[23] H. Habibi and W. O'Connor, "Payload motion control of rotary gantry and luffing cranes using mechanical wave concepts," *Transactions of the Institute of Measurement and Control*, vol. 39, no. 11, pp. 1649–1662, 2017.

[24] H. Ouyang, G. Zhang, L. Mei, X. Deng, and D. Wang, "Load vibration reduction in rotary cranes using robust two-degree-of-freedom control approach," *Advances in Mechanical Engineering*, vol. 8, no. 3, pp. 1–11, 2016.

[25] N. Uchiyama, H. Ouyang, and S. Sano, "Simple rotary crane dynamics modeling and open-loop control for residual load sway suppression by only horizontal boom motion," *Mechatronics*, vol. 23, no. 8, pp. 1223–1236, 2013.

[26] L. A. Tuan, S.-G. Lee, L. C. Nho, and H. M. Cuong, "Robust controls for ship-mounted container cranes with viscoelastic foundation and flexible hoisting cable," *Proceedings of the Institution of Mechanical Engineers, Part I: Journal of Systems and Control Engineering*, vol. 229, no. 7, pp. 662–674, 2015.

[27] W. Singhose, D. Kim, and M. Kenison, "Input shaping control of double-pendulum bridge crane oscillations," *Journal of Dynamic Systems, Measurement, and Control*, vol. 130, no. 3, Article ID 034504, 2008.

[28] Y.-G. Sung and W. E. Singhose, "Robustness analysis of input shaping commands for two-mode flexible systems," *IET Control Theory & Applications*, vol. 3, no. 6, pp. 722–730, 2009.

[29] R. Manning, J. Clement, D. Kim, and W. Singhose, "Dynamics and control of bridge cranes transporting distributed-mass payloads," *Journal of Dynamic Systems, Measurement, and Control*, vol. 132, no. 1, Article ID 014505, 2010.

[30] J. Vaughan, D. Kim, and W. Singhose, "Control of tower cranes with double-pendulum payload dynamics," *IEEE Transactions on Control Systems Technology*, vol. 18, no. 6, pp. 1345–1358, 2010.

[31] E. Maleki and W. Singhose, "Swing dynamics and input-shaping control of human-operated double-pendulum boom cranes," *Journal of Computational and Nonlinear Dynamics*, vol. 7, no. 3, Article ID 031006, 2012.

[32] J. Huang, X. Xie, and Z. Liang, "Control of bridge cranes with distributed-mass payload dynamics," *IEEE/ASME Transactions on Mechatronics*, vol. 20, no. 1, pp. 481–486, 2015.

[33] H. Ouyang, G. Zhang, L. Mei, X. Deng, H. Xi, and D. Wang, "Residual load sway reduction for double-pendulum overhead cranes using simple motion trajectory," in *Proceedings of the IEEE International Conference on Real-Time Computing and Robotics, RCAR 2017*, pp. 327–332, Japan, July 2017.

[34] H. Ouyang, J. Hu, G. Zhang, L. Mei, and X. Deng, "Decoupled linear model and S-shaped curve motion trajectory for load sway reduction control in overhead cranes with double-pendulum effect," *Proceedings of the Institution of Mechanical Engineers, Part C: Journal of Mechanical Engineering Science*, pp. 1–12, 2018.

[35] M. Zhang, X. Ma, X. Rong, X. Tian, and Y. Li, "Error tracking control for underactuated overhead cranes against arbitrary initial payload swing angles," *Mechanical Systems and Signal Processing*, vol. 84, pp. 268–285, 2017.

[36] M. Zhang, X. Ma, X. Rong, R. Song, X. Tian, and Y. Li, "A novel energy-coupling-based control method for double-pendulum overhead cranes with initial control force constraint," *Advances in Mechanical Engineering*, vol. 10, no. 1, pp. 1–13, 2018.

[37] D. Qian, S. Tong, B. Yang, and S. Lee, "Design of simultaneous input-shaping-based SIRMs fuzzy control for double-pendulum-type overhead cranes," *Bulletin of the Polish Academy of Sciences—Technical Sciences*, vol. 63, no. 4, pp. 887–896, 2015.

[38] H. Ouyang, X. Deng, H. Xi, J. Hu, G. Zhang, and L. Mei, "Novel robust controller design for load sway reduction in double-pendulum overhead cranes," *Proceedings of the Institution of Mechanical Engineers, Part C: Journal of Mechanical Engineering Science*, pp. 1–13, 2018.

[39] H. Ouyang, J. Hu, G. Zhang, L. Mei, and X. Deng, "Sliding-mode-based trajectory tracking and load sway suppression control for double-pendulum overhead cranes," *IEEE Access*, vol. 7, pp. 4371–4379, 2019.

[40] H. Ouyang, J. Wang, G. Zhang, L. Mei, and X. Deng, "Novel adaptive hierarchical sliding mode control for trajectory tracking and load sway rejection in double-pendulum overhead cranes," *IEEE Access*, vol. 7, pp. 10353–10361, 2019.

[41] N. Sun, T. Yang, Y. Fang, Y. Wu, and H. Chen, "Transportation control of double-pendulum cranes with a nonlinear quasi-pid scheme: design and experiments," *IEEE Transactions on Systems, Man, and Cybernetics: Systems*, pp. 1–11, 2018.

[42] N. Sun, Y. Wu, Y. Fang, and H. Chen, "Nonlinear antiswing control for crane systems with double-pendulum swing effects and uncertain parameters: design and experiments," *IEEE Transactions on Automation Science and Engineering*, vol. 15, no. 3, pp. 1413–1422, 2018.

[43] S. Sano, H. Ouyang, H. Yamashita, and N. Uchiyama, "LMI approach to robust control of rotary cranes under load sway frequency variance," *Journal of System Design and Dynamics*, vol. 5, no. 7, pp. 1402–1417, 2011.

[44] N. Uchiyama, "Robust control of rotary crane by partial-state feedback with integrator," *Mechatronics*, vol. 19, no. 8, pp. 1294–1302, 2009.

[45] N. Uchiyama, "Robust control for overhead cranes by partial state feedback," *Proceedings of the Institution of Mechanical Engineers, Part I: Journal of Systems and Control Engineering*, vol. 223, no. 4, pp. 575–580, 2009.

[46] C. J. Kempf and S. Kobayashi, "Disturbance observer and feedforward design for a high-speed direct-drive positioning table," *IEEE Transactions on Control Systems Technology*, vol. 7, no. 5, pp. 513–526, 1999.

[47] H. Kobayashi, S. Katsura, and K. Ohnishi, "An analysis of parameter variations of disturbance observer for motion control," *IEEE Transactions on Industrial Electronics*, vol. 54, no. 6, pp. 3413–3421, 2007.

[48] Y. Maeta and M. Iwasaki, "Initial friction compensation by disturbance observer based on rolling friction model," *IEEJ Transactions on Sensors and Micromachines*, vol. 130, no. 2, pp. 3124–3129, 2009.

[49] Z. Masoud, K. Alhazza, E. Abu-Nada, and M. Majeed, "A hybrid command-shaper for double-pendulum overhead cranes," *Journal of Vibration and Control*, vol. 20, no. 1, pp. 24–37, 2014.

[50] M. Chilali and P. Gahinet, "H_∞ design with pole placement constraints: an LMI approach," *IEEE Transactions on Automatic Control*, vol. 41, no. 3, pp. 358–367, 1996.